The current issue and full text archive of this journal is available at
www.emeraldinsight.com/1573-6105.htm

Combined musculoskeletal dynamics/structural finite element analysis of femur physiological loads during walking

Received 2 April 2010
Revised 3 July 2010
Accepted 15 July 2010

David W. Wagner, Kaan Divringi and Can Ozcan
Ozen Engineering, Sunnyvale, California, USA, and
M. Grujicic, B. Pandurangan and A. Grujicic
Department of Mechanical Engineering and Department of Bioengineering, Clemson University, Clemson, South Caroline, USA

Abstract

Purpose – The aim of this paper is to present and evaluate a methodology for automatically constructing and applying the physiologically-realistic boundary/loading conditions for use in the structural finite element analysis of the femur during various exertion tasks (e.g. gait/walking).

Design/methodology/approach – To obtain physiologically-realistic boundary/loading conditions needed in the femur structural finite element analysis, a whole-body musculoskeletal inverse dynamics analysis is carried out and the resulting muscle forces and joint reaction forces/moments extracted.

Findings – The finite element results obtained are compared with their counterparts available in literature and it is found that the overall agreement is acceptable while the highly automated procedure for the finite element model generation developed in the present work made the analysis fairly easy and computationally highly efficient. Potential sources of errors in the current procedure have been identified and the measures for their mitigation recommended.

Originality/value – The present approach enables a more accurate determination of the physiological loads experienced by the orthopedic implants which can be of great value to implant designers and orthopedic surgeons.

Keywords Musculoskeletal system, Limbs, Loading (physics), Human biology, Structural analysis

Paper type Research paper

1. Introduction

It is generally recognized that the employment of finite element analysis in the biomedical practice may potentially have a number of benefits such as offer additional evidence for clinical diagnosis of osteoporosis (Hernandez and Keaveny, 2006), help guide physical therapy (Frost, 1999), assist the development of more efficient/durable implants (Lee *et al.*, 2004), and help improve the understanding of bone remodeling processes (Doblare and Garcia, 2001). However, due to the current inability to validate the finite element models for biomedical systems, finite element analysis (an accepted practice and well-used method in traditional engineering fields) is not at present being accepted as a viable tool in the clinical environment as well as in the areas of human performance, ergonomics and biomedicine (Anderson *et al.*, 2007; Post, 2004).

Multidiscipline Modeling in Materials and Structures
Vol. 6 No. 4, 2010
pp. 417-437

1573-6105
DOI 10.1108/15736101011095118

Some biomedical researchers take an extreme view and characterize the finite element results as being "inherently false" and these researchers do not advocate the use of these results in clinical practice (Viceconti *et al.*, 2005).

It is well established that the accuracy and the fidelity of the finite element models and analyses depends highly on a number of factors among which are:

- accuracy of the associated geometrical models;
- quality of the meshed models;
- suitability and accuracy of the material models; and
- the knowledge of the nature and the magnitude of the boundary/loading conditions.

Regarding the current use of the finite element methods and analyses within the field of biomedical engineering, the main efforts appear to be focused on developing methods for increasing the accuracy (Taddei *et al.*, 2007) and for automated generation of the geometrical and meshed models (Shim *et al.*, 2007). In particular, computed tomography (CT) scans of individual patients have been used to construct geometrical and meshed models for use in the associated finite element analyses (Keyak *et al.*, 2001; Viceconti *et al.*, 2003; Bitsakos *et al.*, 2005; Lee *et al.*, 2004). CT scans have also been used to extract patient specific, spatially-variant material properties (Lengsfeld *et al.*, 1998; Keyak, 2001; Crawford *et al.*, 2003) further increasing the specificity of individualized geometrical biomedical models. This procedure can be nowadays automated and stream-lined using one of the several commercially available computer packages (e.g. Mimics, Analyze, Osiris) with tomographic reconstruction capabilities. These methods and tools allow for patient-specific information to be utilized in the finite element analyses and differ significantly from the previous approaches, which used to rely on cadaver data or commercially available substitutes/surrogates (Cristofolini *et al.*, 1996; Heiner and Brown, 2001).

In contrast to the geometrical and meshed models which are highly accurate and patient specific, the boundary/loading conditions (i.e. internal body forces) such as muscle forces and joint reaction forces and moments are often not well known and, hence, highly simplified. For example, both laboratory and finite-element structural analyses of the femur are carried out under the conditions in which the femur condyles are fixed while loading is applied to the femur head or at the greater trochanter. This test set-up is often used to determine of bone material properties (Yosibash *et al.*, 2007; Taddei *et al.*, 2007), quantify fracture loads (Cody *et al.*, 1999; Keyak and Falkinstein, 2003), to elucidate bone remodeling processes (Jacobs *et al.*, 1997) and to help improve orthopedic implant designs (Doblare and Garcia, 2001). However, *in vitro* measurements of the axial strains in the long bone of the femur for simplified muscle configurations have been shown to over-estimate, by as much as 44 per cent, strains within the femur relative to those obtained under more physiologically realistic setups (Cristofolini *et al.*, 1996). This finding clearly revealed the extent of sensitivity of the femur structural response to the level of fidelity and accuracy of the physiological loads acting on the femur. The present inability to accurately quantify these physiological loads is, as mentioned earlier, one of the main impedances to a wider utilization of the finite element analyses in the biomedical engineering community and clinical practice.

It is well recognized that when considering more complex loading conditions, realistic muscle models are required in order to accurately represent anatomical configurations. Finite element analyses that use simplified or compartmentalized muscle models have been shown to lead to significant inaccuracies in the finite element results (Taylor *et al.*, 1996; Duda *et al.*, 1998; Speirs *et al.*, 2007). Physiologically, inconsistent femur strain patterns are found to develop when over-simplified finite element models are used which involved less than 16 different muscles (Duda *et al.*, 1998). Duda *et al.* (1998) also reported that changes in the strain magnitudes of the order of 30 per cent could result from the use of overly simplified boundary/loading conditions. In the same study, un-physical bending moments were introduced into the finite element model when highly simplified muscle models are used. These moments were shown to cause increases in the distal femur maximum principal strains in a 50-60 per cent range.

Despite the aforementioned effect of the boundary/loading conditions on the finite element results, many of the published studies simulating femur and hip joint stresses utilize simplified boundary conditions and do not include realistic physiological boundary conditions related to muscular forces (Huiskes and van Rietbergen, 1995; Mann *et al.*, 1997). One exception includes a lower extremity muscle model that has been applied to the gait analysis of one subject (Brand *et al.*, 1982, 1986) has been utilized in several studies (Duda *et al.*, 1998; Bitsakos *et al.*, 2005; Yosibash *et al.*, 2007). Although the use of the same muscle model and its single parameterization may lead to increased reproducibility within research community, this muscle-model singularity may also be associated with a number of shortcomings such as:

- it may lead to difficulties in the application of currently defined muscle models to new human subjects;
- it may be associated with greater complexity in recording the necessary information for analyzing novel exertions; and
- it may suffer from the inability to readily include patient-specific muscle data.

There is currently no generally accepted method for defining boundary/loading conditions for novel exertion (patient-activity) tasks (Erdemir *et al.*, 2007). These limitations are the key obstacles to carrying out comparative finite element analyses involving a single subject performing multiple tasks or a group of subjects performing the same task. The main objective of the present work is to demonstrate how the use of a whole-body musculoskeletal inverse dynamics analysis can provide the needed physiologically-realistic boundary/loading conditions associated with different exertion tasks.

As recently demonstrated by Grujicic *et al.* (2009, 2010a, b, c, d), musculoskeletal inverse dynamics analysis offers a potential solution for producing detailed boundary/loading conditions over a wide range of body movements. This type of analysis is rigid-body based and enables computation of the muscle and joint reaction forces necessary to replicate complex body motions (Koopman *et al.*, 1995; Anderson and Pandy, 2001; Damsgaard *et al.*, 2006; Ren *et al.*, 2007). Inverse dynamic musculoskeletal models are commonly driven by kinematic data of actual human movements and used to estimate internal body muscle forces, which are difficult, if not impossible, to measure directly. Particularly in conditions with irregular motions or positions, inverse dynamics analysis can be a useful tool for quantifying muscle activation patterns (Stokes and Gardner-Morse, 2004).

The AnyBody (Anybody Group, Aalborg, Denmark) modeling software was used in the present work as the inverse dynamics analysis solver. Although similar commercially available solvers exist (e.g. LifeModeler, San Clemente, California; Musculographics, Chicago, Illinois; SAM, Marlbrook Ltd), the AnyBody software was chosen to facilitate the desire for minimal definition by the user to construct the finite element bone model boundary/loading conditions. The AnyBody software includes readily available body and application models in which the kinematic constraints, muscle geometry and prescribed movements required for performing a musculoskeletal simulation are already defined (Rasmussen *et al.*, 2003). The AnyBody software utilizes an optimization scheme that can be interpreted as a "minimum effort" criteria to solve for the redundant muscle forces used for actuating equivalent kinematics of the system (Damsgaard *et al.*, 2006). A precompiled AnyBody application model of gait/walking along a straight path was used in the present work as the task for which the finite element model boundary conditions were computed (Rasmussen, 2006).

As mentioned earlier, for the finite element models and analyses to attain a wide spread use in the broader biomedical community and in the clinical practice, they need to be accessible to users who may not be experts in the areas of biology, computational mechanics and/or finite element simulation. By utilizing validated inverse dynamics-based musculoskeletal models for automatically defining the boundary/loading conditions, finite element models/analyses can be readily formulated for internal body structures undergoing realistic exertions. The realization of such a process may have widespread consequences such as:

- development of suitably acceptable finite element models for use in the clinical environment;
- an improved assessment of bone health through the automation and incorporation of finite element analysis with conventional bone scanning technology (Lengsfeld *et al.*, 1998; Cody *et al.*, 1999; Crawford *et al.*, 2003);
- improvements in bone-fracture prediction (Keyak *et al.*, 2001; Doblare and Garcia, 2003);
- the prediction of bone remodeling processes (Jacobs *et al.*, 1997; Stülpner *et al.*, 1997; Doblare and Garcia, 2001), which could be controlled/affected by physical therapy (Frost, 1999; Heaney, 2003);
- pain management through implant design optimization (Lee *et al.*, 2004); and
- assessment of the fracture fixation and bone-healing promotion efficacies of the orthopedic implants (Bergmann *et al.*, 1995; Schneider *et al.*, 2001; Lee *et al.*, 2004; Grujicic *et al.*, 2010a, b, c, d).

With continuously increasing computational power and its affordability, the main impediment for the development of high fidelity/accuracy biomedical finite element models is not to computationally solve these complex models, but the ability to attain the required level of physical realism in these models. Within the present work, a procedure is developed for automatically extracting the results from a whole-body-based musculoskeletal simulation to define the boundary conditions for a finite element model of a bone segment. The methodology is applied to analyzing the strains, stresses and deformations of a femur during a nominal gait cycle. The simulation results are compared with their counterparts obtained in previous studies.

2. Materials and methods

As mentioned earlier, a detailed structural finite element analysis of the femur associated with normal walking of a human subject is carried out in the present work. It was also mentioned that in order to generate physiologically-realistic boundary/loading conditions experienced by the femur, a whole-body musculoskeletal analysis had to be carried out. In this section, details of the finite element and the musculoskeletal inverse dynamics analyses are presented.

2.1 Meshed model generation procedure

A finite element meshed model of a human femur was created using Mimics v12 (Materialise, Leuven, Belgium). The femur anatomy was based on CT scan data included with the Mimics tutorial software. The femur was 41 cm long with a maximum width of 5.4 cm at the condyles. The CT scan data used had a resolution of 0.684 mm and were associated with planar sections at 1.5 mm intervals. A mesh consisting of the first order tetrahedral elements with an average edge-length of $\sim$2 mm was generated and subsequently imported into ANSYS Workbench v11 (ANSYS Inc, Canonsburg, Pennsylvania). The complete model of the human femur consisted of 89,891 tetrahedral elements (Ansys Element Type, Solid185 – 4 node linear tet) with 18,497 nodes. Thereafter, the finite element analysis is solved using a dual-core AMD Opteron Windows XP 64-bit workstation.

2.2 Assignment of the bone material properties

Owing to a lack of calibration data for the CT scan, the material property of each tetrahedral element was defined using a procedure similar to that used by Peng *et al.* (2006). The densities were assigned by linear interpolation between 100 and 2,000 kg/m^3 and correlated with a range of Hounsfield Units (HU) determined from the CT scan. The HU of each voxel in the CT scan indicates the radiodensity of the material, distinguishing the different bone tissue types. Figure 1(a) shows the distribution of HU among the voxels of the femur. The maximum HU of the CT scan, 1,575, was defined to be the hardest cortical bone of density (2,000 kg/m^3) and the HU value of 100 were defined to be the minimum density of cortical bone (100 kg/m^3). A total of 400 unique material properties were defined using the CT scan data to model the femur bone (Figure 1(b)). The extracted material properties were modeled as linear elastic and isotropic. Elements with a HU of below 100 were merged into a uniform intramedullar tissue element type and assigned an elastic modulus of 20 MPa. The remaining 399 elements were assigned elastic moduli calculated from apparent densities using axial loading equations developed by Lotz *et al.* (1991), with a HU of 801 and above defined as cortical bone ($E = 2{,}065\rho^{*}3.09$ MPa) and a HU of 800 and below defined as cancellous bone ($E = 1{,}904\rho^{*}1.64$ MPa). A Poisson's ratio of 0.30 was used for all materials. Figure 2 shows the general distribution of material properties for the femur bone.

2.3 Musculoskeletal model and analysis

As discussed earlier, in order to generate physiologically-correct boundary/loading conditions needed in the finite element analysis of the femur, a whole-body musculoskeletal analysis of the gait had to be carried out first. In the remainder of this section, a brief account is given of the musculoskeletal model and the analysis employed.

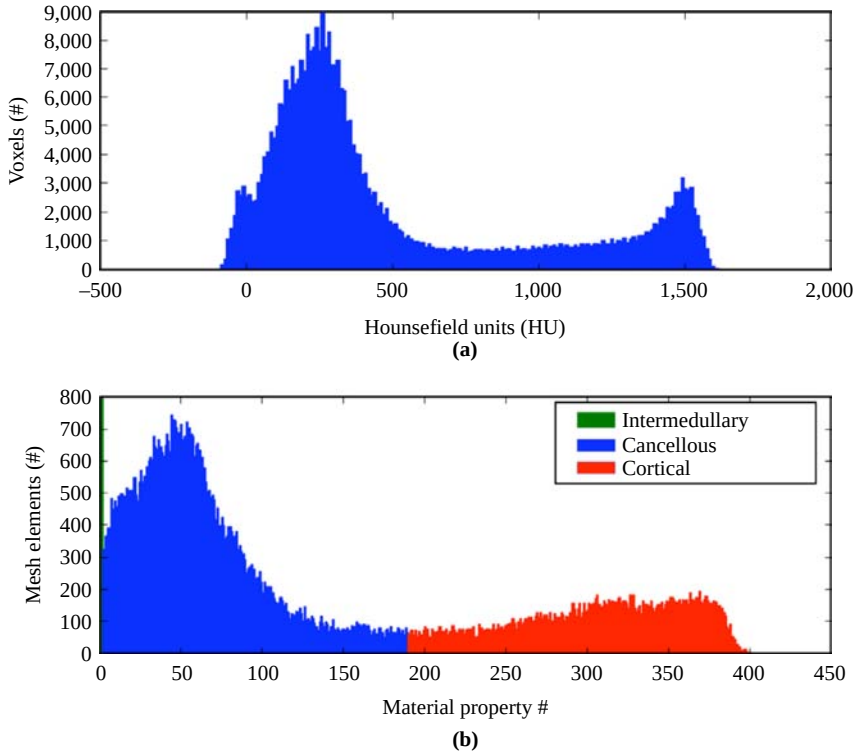

Figure 1.
(a) The HU and accompanying number of voxels in the femur calculated from the CT scan by Mimics and (b) the 400 material property types and the associated number of elements

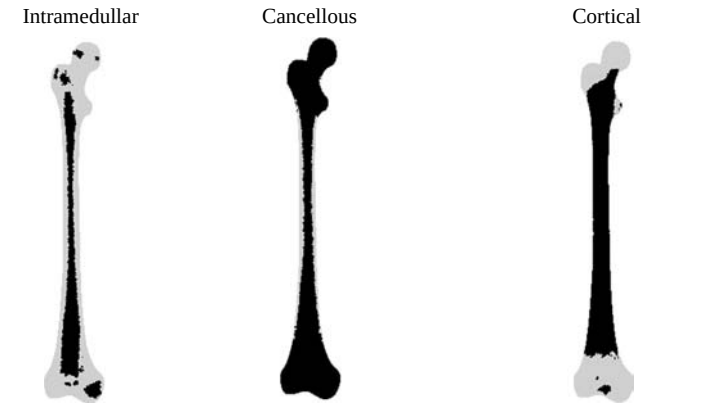

Note: Included elements are shown in black

Figure 2.
Distribution of elements with the three major categories of material properties in the femur bone and corresponding ranges of Young's modulus and density

The kinematics and external forces used as input to drive the AnyBody model gait study under investigation were derived from a previous gait analysis study (Vaughan *et al.*, 1992). The procedure used to define the boundary conditions was independent of the gait study application presented here. The AnyBody musculoskeletal model used in this analysis is available in the AnyBody Repository v7.0 (in the "/Application/Validation/GaitVaughan/" folder). To facilitate comparison with previous studies (Duda *et al.*, 1998; Bitsakos *et al.*, 2005), four stages in the gait cycle were chosen for analysis (Figure 3). The four specific times in the gait cycle used for analysis (9, 47, 55 and 82 per cent) were selected using the same criteria as Duda *et al.* (1998). Although the specific times in the gait cycle used by Duda *et al.* (1998) were available (30, 45, 10 and 70 per cent) in the current analysis, they were deemed to be not directly associated (by kinematics or kinetics) to the gait pattern used here. Instead, the same justifications used by Duda *et al.* (1998) in the selection of relevant time steps were used here to determine comparable time steps. The 9 and 47 per cent stages in the analyzed gait cycle correspond to the first and second peaks in ground reaction forces (GRFs) (30 and 45 per cent of the gait cycle presented by Duda *et al.* (1998)). The instant of maximum muscle activity (55 per cent of the gait cycle for the presented study) was calculated using the AnyBody model and corresponded to the peak activity of the soleus muscle. The 82 per cent time step of the gait cycle corresponds to the swing phase of the right lower extremity.

The rigid body AnyBody femur model consisted of 28 connected "via-point" muscles and one wrapped muscle that was used to model the Iliopsoas muscle group. All the muscles were defined with an origin and insertion point. The via-point muscles also included between zero and three intermediate points, which were used to constrain the path of the muscle. The intermediate via-points are defined with respect to the local coordinate system of the bone, similar to the origin and insertion points. The via-points can be interpreted as a point the muscle passes through that constrains the muscle path to the via-point (i.e. the muscle can slide through the via-point). The force transmitted

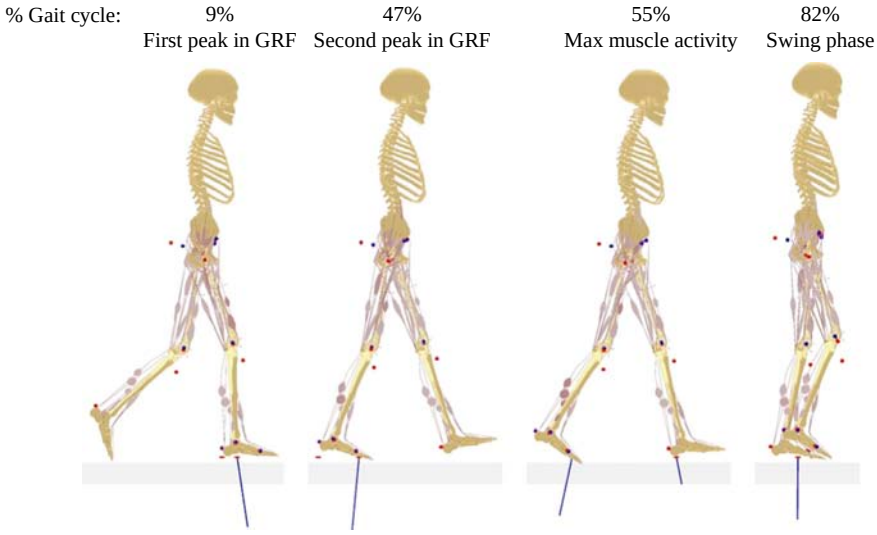

Note: The blue line(s) represents the force, and point of application, of the GRF for each time step

Figure 3.
The AnyBody model gait application at the four time steps considered in this study

to the bone due to the muscles connected by origin or insertion points is directed along the muscle path while the force transmitted to the bone due to the muscles connected by via-points is directed perpendicular to the path of the muscle. The paths of the muscles between the origin, via-points and insertion points are modeled as straight lines in the AnyBody Modeling System. The Iliopsoas muscle was discretized into 50 individual straight-line muscle segments and wrapped about a geometric cylinder used to approximate the anatomical surface the muscle path follows. All the muscles were modeled as three element hill-type muscles with the default parameters defined in the AnyBody Repository v7.0 (www.anybody.aau.dk/repository/Repository7.0/index.htm). Table I documents the AnyBody femur muscle model and compares it to previous muscle models used for FE applications in the literature.

2.4 Definition of the boundary/loading conditions

The location of the muscle force application points on the finite element femur model were calculated using the anatomical representation of the corresponding nodal positions used in the AnyBody musculoskeletal body model. The finite element model of the femur (derived from CT scan data) was scaled and oriented to match the rigid body representation of the AnyBody femur. The nodal positions defined in AnyBody were used to match identifiable bony landmarks on the finite element model. An automated process was utilized in which the finite element model was:

- uniformly scaled to match selected nodal distances of the rigid body model; and
- reoriented to align the corresponding nodal positions of both models. Several iterations using different nodal sets were performed.

Owing to the differences in anatomical definitions, the AnyBody nodes that were used to define the points of force application could not be perfectly aligned with the nodes or surface of the finite element geometry. A second automated procedure was then used to re-define the AnyBody nodal positions of the musculoskeletal model to the closest (by Euclidean distance) finite element model surface node (Figure 4). The average displacement of the AnyBody femur nodes to be coincident with the surface of the finite element model was 0.0011 m. The maximum displacement of the 30 femur nodes was for the intermediate (via-point) node of the Sartorius muscle at 0.0038 m.

The forces applied to each individual node of the finite element model were equally distributed to the surface nodes connected to the tetrahedral elements that the individual node was connected to limit the probability that the applied forces would result in a singularity. Figure 5 shows the forces and application points on the right femur at the time of the first peak in the GRF (9 per cent of the gait cycle).

The automated procedure developed as part of the present work, allowed for the muscle forces to be applied at the same positions in both the AnyBody model and the finite element model while maintaining the force equilibrium. Specifically, information regarding the position of the muscle attachment points obtained from AnyBody was used to construct finite element reference nodes for couplings lying on the outer surface of the femur. Next the muscle forces obtained from AnyBody were applied to the reference nodes while the couplings ensured that these forces do not create unphysical/stress-concentration effects at the muscle attachment locations. The joint reaction forces at the hip and knee (Table II) were applied to the finite element model in a similar manner as described for the muscle forces. Since the sum of the muscle forces

Boundary condition	AnyBody	Taylor *et al.* (1996)	Duda *et al.* (1998)
Hip joint reaction	X	X	X
Knee joint reaction	X	(constrained)	X
Gastrocnemius			
Lateralis	X		X
Medialis			X
Vastus			
Lateralis	X		X
Medialis	X		X
Intermedius	X		X
Gluteus			
Minimus	X	X[a]	X
Medius	X		X
Maximus			
1	X		
2	X		X
3	X		
Illiotibial tract	X[b]	X	
Tensor Fasciae			
Latea	X		X
Adductor			
Longus	X		X
Magnus			
1	X		
2	X		X
3	X		
Brevis	X		X
Illiopsoas	X	X	
Vastus			
Lateralis	X		X
Medialis	X		X
Intermedius	X		X
Biceps Femoris			
Brevis	X		X
Sartorius	X[b]		
Pectineus	X		X
Quadratus Femoris	X		
Obturatorius			
Externus	X		
Internus	X		
Gemellus			
Superior	X		X
Inferior	X		
Piriformis	X		
Popliteus			
Psoas Major (Iliopsoas)	X		X
Iliacus (Iliopsoas)			
Patellar interactions			X

Notes: Merged cells indicate muscles that were simplified and combined into a single boundary condition; [a]referred to as "abductors" but placement and orientation most closely matches gluteus minimus; [b]implemented as a via-point (i.e. intermediate point of a muscle path)

Table I. Comparison of the AnyBody lower extremity muscle model and two models from the literature used in similar studies (Taylor *et al.*, 1996; Duda *et al.*, 1998) to define the boundary conditions to the femur for finite element analysis

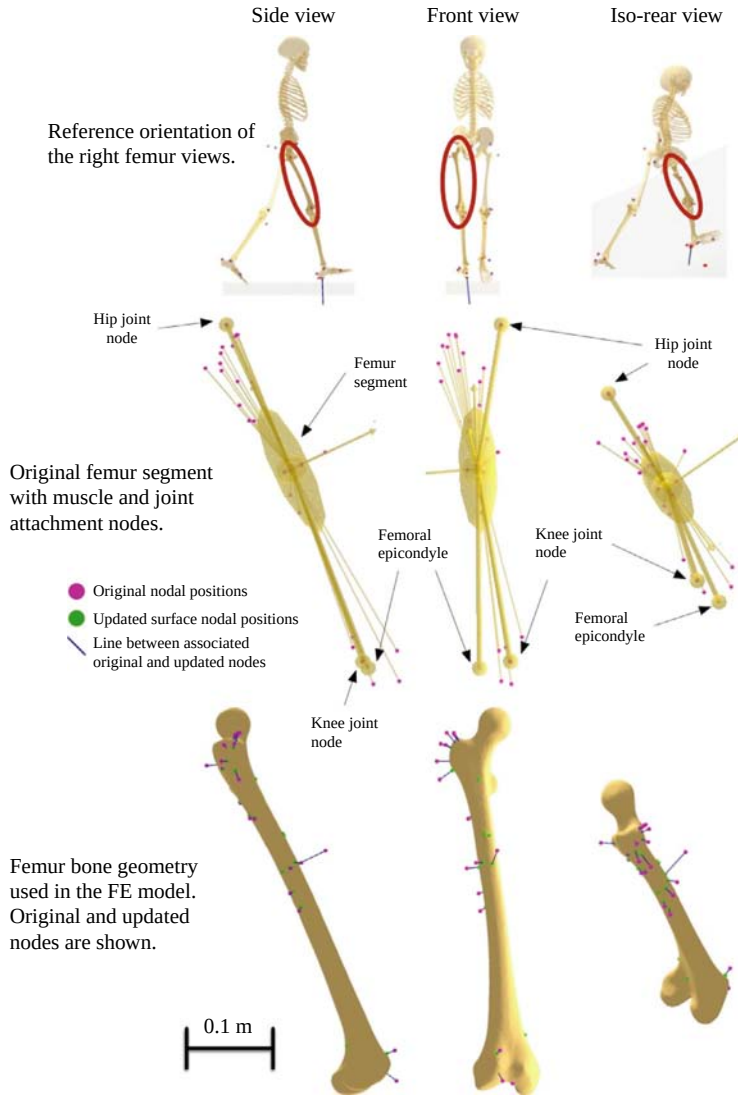

Figure 4.
Original (AnyBody defined) and updated (constrained to the surface of the femur geometry) node positions for the right femur

and joint reactions were in equilibrium, there was no need to artificially constrain the position of any node or geometry feature of the finite element model. However, to suppress rigid body motion caused by numerical error, the finite element model was supported by weak springs. While one end of each of these springs was attached to the femur, the other end was fixed.

3. Results

The key structural finite element results obtained in the present work are presented and analyzed in this section. Since these results involved spatial distributions of the

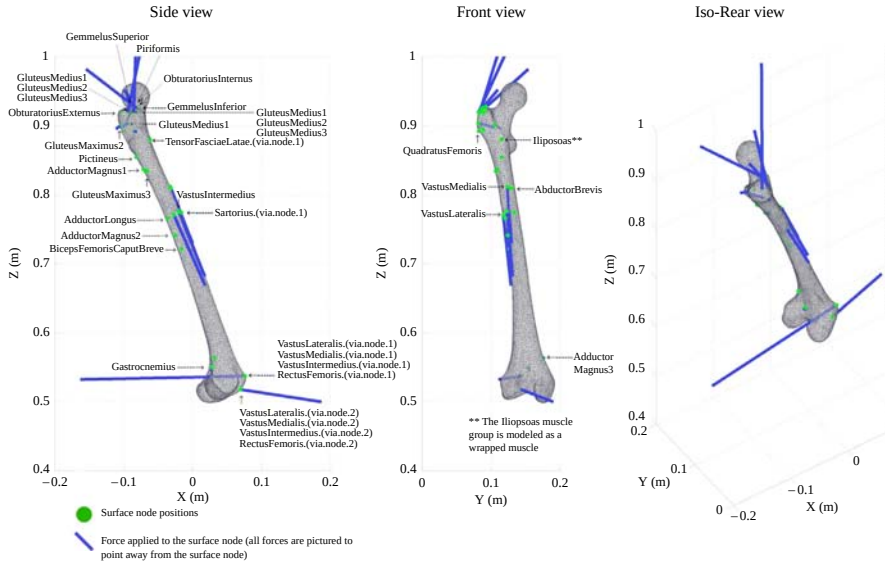

Figure 5.
Muscle forces directions, relative magnitudes, and application points (labeled) for the right femur at the time of the first peak in GRF (9 per cent in the gait cycle)

Table II.
Resultant joint reaction force magnitudes at the hip and knee joint simulated by the AnyBody model for the four gait time steps analyzed

Resultant joint percentage reaction magnitude	Gait cycle 9% (first peak in GRF)	47% (second peak in GRF)	55% (max muscle activity)	82% (swing phase)
Hip force (N)	2,378	3,075	2,027	173
Knee force (N)	2,115	1,811	1,485	111

strains, stresses and deformations/deflections during the gait cycle, this section is structured accordingly.

3.1 Strain distributions

The maximum principal strains in the long bone of the femur, defined here as the section of bone located between the lesser trochanter and a point 6 cm proximal of the epicondyles, are presented. This section of the bone corresponds to approximately where the cortical bone completely wraps the surface of the femur (Figure 2). A peak strain of 5,400 με (microstrains) occurred over the four time steps analyzed at the second peak in GRF (47 per cent of the gait cycle) at a location four centimeters distal of the lesser trochanter of the femur. Similar relative strain distributions were observed for the three time steps of 9, 47 and 55 per cent of the gait cycle with the maximum strains occurring for the 9 and 55 per cent gait cycle time steps at approximately the same location as the 55 per cent gait cycle with values of 5,300 and 4,200 με, respectively. The strains of the femur during the swing phase (82 per cent of the gait cycle) did not result in values greater than 208 με. The relative strain magnitudes along the long-axis surfaces of the femur bone were dependent on the time step of the gait cycle analyzed, particularly for the anterior surface. The strains (max principal) along the anterior, posterior, medial and

lateral sides of the long-axis of the femur bone are plotted in Figure 6. The strain data for each side was calculated on paths manually defined along the edges between elements in the finite element mesh. The strain distribution for each surface exhibited the same trend between the time steps analyzed, for which the right foot was in contact with the ground, with the exception of the anterior surface strain. The anterior surface strain of the first peak in GRF increased from the distal to proximal end of the femur from ~250 to ~1,100 με while the strain from the other two time steps with the right foot in contact with the ground remained consistent over the length of the bone with the majority of strains being under 500 με. A general trend most pronounced on the lateral surface and to a lesser extent on the medial surface, where the strain increased from the distal to the proximal end of the bone was observed, potentially caused by a larger number of active muscles connected to the proximal end of the femur causing the localized expansion. The lateral surface strain increased from ~1,000 to ~4,000 με (on average for the right foot ground contact time steps) from the most distal to the most proximal portion of the long bone. The strains observed on the lateral surface of the proximal side of the bone were two times larger than the strains on the same side of the bone for the medial surface, and four times as large as the anterior and posterior strains.

3.2 Stress distributions

During the time steps the right foot was in contact with the ground (9, 47 and 55 per cent of the gait cycle) the resulting von Mises stresses on the medial surface of the right femur bone were observed to be significantly higher than on the remaining surfaces (Figure 7). For the same time steps, a high stress region was also observed at a

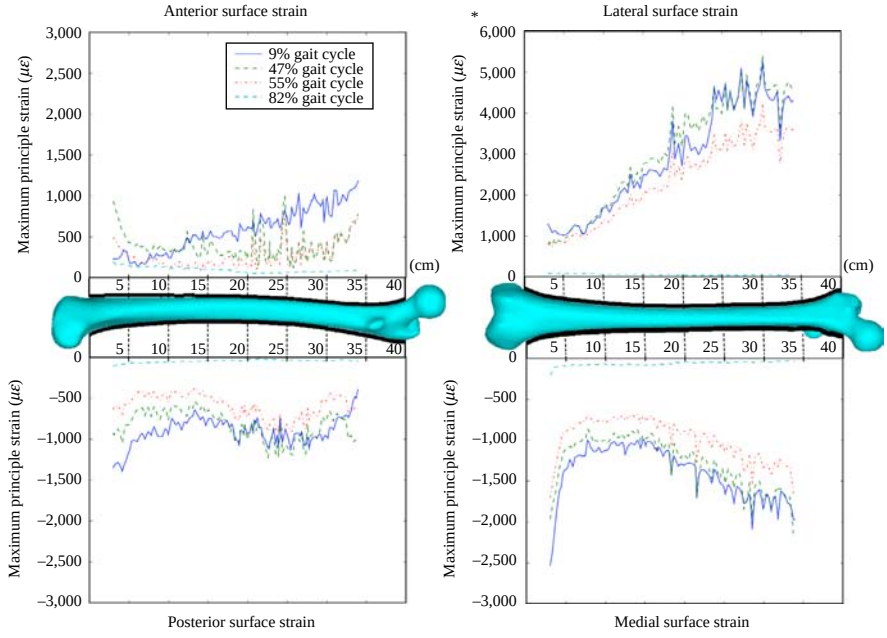

Note: The x-axis of each graph corresponds with the position on the closest edge of the femur pictured above or below it

Figure 6.
Surface maximum principal strains along four facing edges of the femur

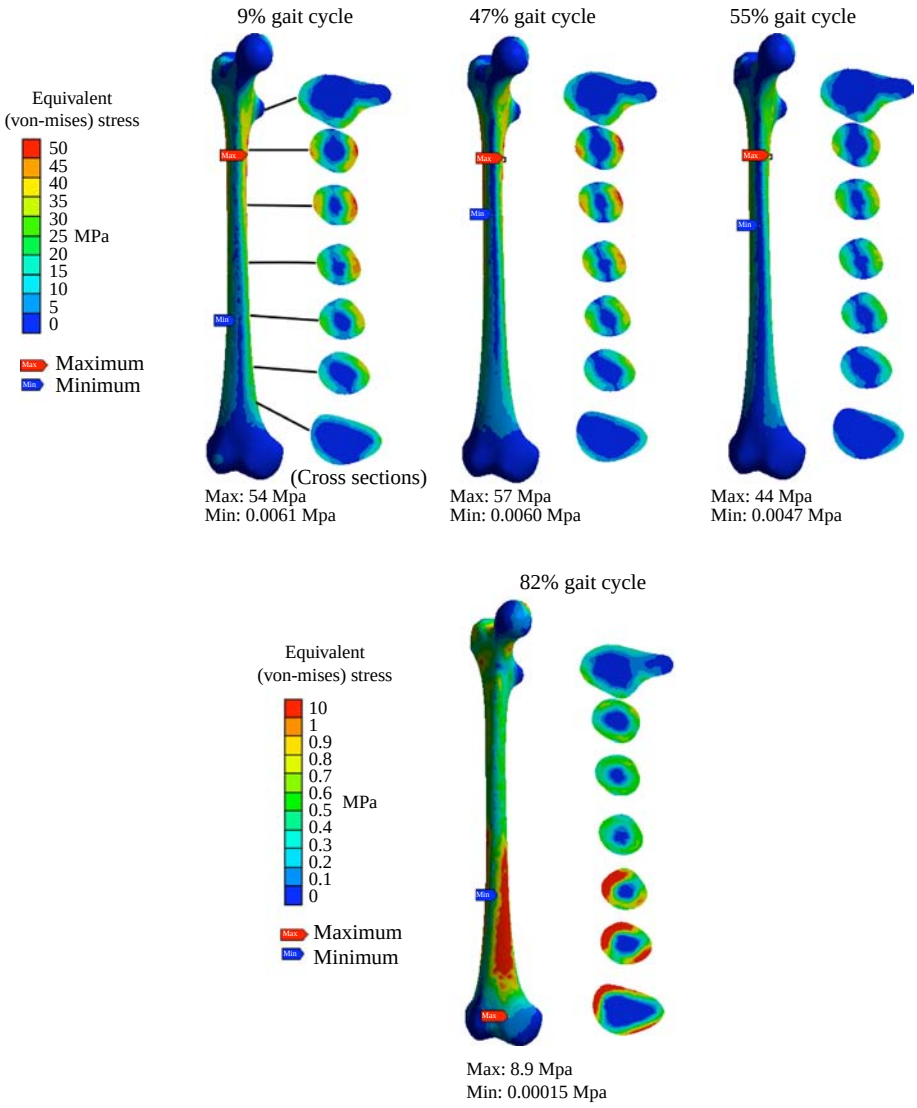

Note: Maximum and minimum stresses are indicated at each percentage of the gait cycle

Figure 7.
Stresses (von Mises) along the full femur and selected cross-sections of the femur

location slightly distal of the lesser trochanter extending halfway down the long axis of the bone. The high stress region included the maximum stresses observed for the 9, 47 and 55 per cent of the gait cycle time steps corresponding to 54, 57 and 44 MPa, respectively. In contrast, during the swing phase (at 82 per cent of the gait cycle) the lateral surface showed the majority of the higher magnitude stresses throughout the femur bone. However, all the stresses for the swing phase remained under 9 MPa.

Axial cross-sections of the long-axis of femur were analyzed to determine the stress gradients between the different surfaces of the bone. At the second peak in GRF (47 per cent of the gait cycle) the stresses in an axial cross-section located four centimeters distal of the lesser trochanter resulted in a gradient with a maximum stress of 54 MPa on the medial surface of the bone, a maximum stress of 47 MPa on the opposing lateral surface and a minimum stress of 23 kPa in the intermediate intramedullary tissue. Similar trends in the axial stress gradients were observed progressing distally along the bone away from the hip joint with increasing reductions in stress magnitudes for both the medial and lateral stresses at each axial cross-section taken suggesting a higher concentrated loading closer to the hip joint than the knee joint. Similar trends in the axial gradients were also observed between the time steps with the right foot in contact with the ground. However, the maximum medial and lateral surface stresses were also reduced for corresponding axial cross-sections. For example, the maximum medial and lateral surface stress at the first peak in GRF (9 per cent of the gait cycle) time step for the same cross section as defined for the second peak in GRF (see above) was 4 and 3 MPa lower, respectively. The difference between the medial and lateral surface stresses decreased to 5 MPa for the maximum muscle activity time step (55 per cent of the gait cycle), with a maximum of 41 MPa on the medial surface and a minimum of 18 kPa in the intramedullary tissue. During the swing phase (82 per cent of the gait cycle), the stress difference in the axial cross-section located near the distal end of the bone (11 cm from the epicondyles) ranged between 1.4 and 2.3 MPa on the medial and lateral surfaces, respectively, with a minimum of 0.34 kPa in the intermediate intramedullary tissue.

A stress gradient was also observed between the adjacent anterior/lateral and posterior/medial surfaces. A surface stress gradient of 42 MPa was observed between the maximum medial surface stress of 49 MPa and the minimum posterior surface stress of 7.0 MPa for the an axial cross-section located 11 cm distal of the lesser trochanter for the 9 per cent gait cycle time step. At the second peak in GRF, the same surface gradient increased to 45 MPa, with a maximum medial stress of 47 MPa. At the instant of maximum muscle activity, the same surface gradient decreased to 31 MPa, primarily due to the decrease in the peak medial surface stress to a value of 34 MPa. For the same cross section, the anterior/lateral gradients were lower at 28, 36 and 26 MPa at 9, 45 and 55 per cent of the gait cycle, respectively.

3.3 Deformation/deflection distributions

Deformations of the femur for the gait time steps with the right foot in contact with the ground revealed significant deflections in the mid-bone (Figure 8). The maximum total deformation (47 per cent of the gait cycle) corresponded to the time step for which the full body weight of the subject was supported on one leg. The majority of bone deflection was observed toward the lateral direction (in the coronal plane) with deflections of 8.9, 9.2 and 7.1 mm for the 9, 47 and 52 per cent gait cycle time steps, respectively. As correctly pointed out by one of the reviewers of this manuscript, these values appear to be somewhat excessive. This finding may suggest that the bone stiffness values used may be too low. The deflections in the sagittal plane were 2.7, 3.7 and 2.4 mm in the anterior direction and 2.5, 2.7 and 2.0 mm in the proximal direction for the 9, 47 and 52 per cent gait cycle time steps, respectively. The maximum point of deformation for each time step occurred at a point along the long bone close to where

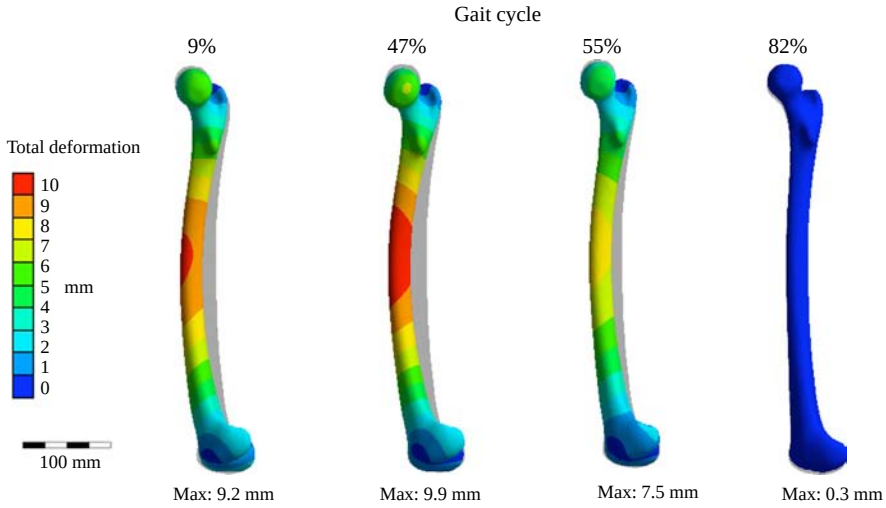

Note: The deformations of the rendered bones are exaggerated 5× for illustrative purposes

Figure 8.
Deformations of the femur at four points in the gait cycle, overlaid with the un-deformed bone in gray

the natural curvature of the bone changes inflection in the coronal plane. In the swing phase (at 82 per cent of the gait cycle) the components of the deflection were approximately equal at 0.2 mm and positive in the directions considered previously.

4. Discussion

The aim of this study was to present and evaluate a generic methodology for defining a finite element model of a bone, subjected to internal body loads that corresponded to a novel exertion. The methodology was evaluated in the present work for a finite element model of a femur bone over four time steps of a gait cycle. The finite element model of a femur bone was derived from CT scan data. Mass and inertia properties calculated from the finite element femur model were used in the musculoskeletal simulation. The muscle insertion points and paths from the musculoskeletal model were scaled to match the geometry of the femur bone. Muscle and joint reaction forces were determined for four time steps in a gait cycle corresponding to the two peaks in GRF, maximum muscle activity and the swing phase. Maximum principal strain, von Mises stress and total deformation along the surface of the long axis of the femur bone were analyzed.

One of the main objectives of the present work was to develop a generic software tool that automatically streamlines the procedure for defining the boundary/loading conditions of finite element models for simulating internal body structure stresses and strains for novel exertions. Such a tool was developed and its trial version can be accessed at www.ozeninc.com/Any2Ans.

A comparison of the results obtained in the present work with their counterparts reported in the literature established the following:

- The maximum principal strains along the long axis of the femur bone showed mixed resemblance with the results presented by Duda *et al.* (1998) for a similar muscle loading condition and time in the gait cycle (corresponding to the second peak in GRF) for a left femur. The maximum principal strains showed similar trends

between the two studies along the medial and anterior surfaces with the peak strains being located along the medial surface in the subtrochanteric region for both studies. The magnitude of the strains along the anterior surface for both studies was also relatively homogeneous at approximately 500 με. Taylor *et al.* (1996) reported maximum medial strains in the axial direction below −1,500 με with the majority of bone having less than −1,000 με. The medial surface strain results presented in the present work were slightly higher, possibly due to the maximum principal strains not being directly aligned with the axial direction. Speirs *et al.* (2007) presented maximum principal strains along the long-axis of a femur under "physiological constraints" (case E) for a time step during a gait stride for which the maximum hip reaction forces were observed. The anterior surface strains were similarly the lowest in average magnitude across all the surfaces for both studies, however the posterior strains presented in this work were approximately one-third the magnitude of those presented by Speirs *et al.* (2007). Although the lateral surface strain presented here exhibited the same trend (increasing in a linear manner from the distal diaphyseal to the intertrochanteric level) as those presented by Speirs *et al.* (2007), the magnitude was also approximately twice as large suggesting the femur presented in the present work exhibited more bending in the coronal plane. Schileo *et al.* (2007) applied 15 strain gauges to the surface of eight femurs placed in a mechanical test rig and reported maximum principal strains for all gauges to be approximately between 1,000 and −1,000 με. Several loading conditions were applied, although all used the same force magnitude of 75 per cent of the femur donor's body weight, which may be one reason why the strain magnitudes were significantly less than those reported in the present work.

- The von Mises stress gradients between the medial/lateral and anterior/posterior surfaces obtained in the present work were not uniform as suggested by Taylor *et al.* (1996) for physiological loading conditions. Taylor *et al.* (1996) observed similar results for initial loading cases and were able to generate more uniform stress distributions by increasing the angle of the applied hip reaction force to 20° from vertical. The intent of this paper was to evaluate a currently available musculoskeletal model for defining the boundary conditions of a finite element model and as such, changes to the calculated forces were not investigated to replicate one particular set of results. One potential explanation to this discrepancy of non-uniform stresses may be that the application of the hip reaction force to the femur in the current AnyBody leg model may deviate from the reaction force angle suggested by Taylor *et al.* (1996). However, as the reaction force at the hip has been validated against other measurements (Rasmussen, 2006), a more likely reason may be attributed to the manual procedure used to align the femur bone to the AnyBody nodal landmarks. A different set of nodal coordinates used to align the femur geometry or a more cohesive definition between the femur geometry and the rigid body nodes may reduce the stress discrepancy discussed here.
- A similar comparison of the deformations of the femur model presented here to the previously mentioned finite element models revealed similar comparisons. The automated procedure presented here for defining boundary conditions had smaller deflections than the finite element models with constraints not specifically defined to be physiologically consistent (Taylor *et al.*, 1996; Speirs *et al.*, 2007), but still had a greater magnitude of deflection (at the mid-bone) than the corresponding

physiologically constrained models. For the physiological boundary constraint, Speirs *et al.* (2007) explicitly observed a lateral bow of the femur, similar to the deformation presented here. The difference in the magnitude of the applied hip reaction force was minimal (75 N) between the model presented here (for the second peak in GRF) and that presented by Taylor *et al.* (1996). However, the elastic modulus used by Taylor *et al.* (1996), particularly to model the cortical bone (17,000 MPa), was significantly higher than the range of values used in the present work (ranging from 1,850 to 16,737 MPa). Speirs *et al.* (2007) used the same cortical bone elastic modulus as Taylor *et al.* (1996), in addition to assigning a value of 1,000 MPa for the cancellous bone elements, while the corresponding values used in the present work ranged from 77 to 1,835 MPa. The higher elastic modulus used by Taylor *et al.* (1996) and Speirs *et al.* (2007), particularly for the cortical bone, would result in a stiffer femur than the one used in the present work and potentially explain the smaller observed overall deflections in those respective studies.

- One additional factor that affected the results presented in the present work was the methodology used to generate the material properties, particularly of the cortical bone. The relationship between the elastic modulus and the HU (Peng *et al.*, 2006) developed by linearly relating HU to apparent density seems to have resulted in particularly low values of elastic moduli when compared to other models in literature (Wirtz *et al.*, 2000). The range of HU used in this study yields an elastic modulus an order of magnitude smaller at lower HU values when compared to other models (Yosibash *et al.*, 2007). In retrospect, the linear interpolation of apparent density from HUs may have been too simplified to yield a good representation of apparent density for the CT-scan. The resultant effect in the model was that the cancellous bone did not share the load evenly with the area of cortical bones, introducing singularities at muscle attachment points and increases in strains from the cortical areas. Further investigation and integration of new methods for defining material properties (Yosibash *et al.*, 2007) may help in reducing errors of the presented methodology for future applications.

One fundamental limitation of the proposed methodology included an inability to directly validate the developed finite element model with a physical test specimen. Unfortunately, the capacity to directly measure femur strains, stresses, or deformations for individual subjects performing dynamic tasks is highly prohibitive. However, the results were evaluated against several similar studies with related boundary conditions in an attempt to provide an element of consensus validity to the methodology presented here through the derived results. Several assumptions were made in the process of implementing the procedure for automatically applying the predicted muscle forces to a finite element model that should be highlighted. The procedure for displacing the rigid body defined nodes to be coincident with the bone geometry was assumed to not significantly affect the anatomical definitions validated in the musculoskeletal model in a negative fashion. The manual procedure for aligning the bone geometry to the un-displaced node positions was performed in an *ad hoc* manner and was assumed to not have introduced significant errors associated with misaligned geometry, although as previously mentioned, may have resulted in higher femur stresses.

In summary, the automated procedure described in this paper for incorporating simulated muscle forces as boundary/loading conditions to a patient-specific finite

element femur model was used to compare the strains, stresses and deformations along the long axis of the bone with other published results. Although a perfect match was not found between the results presented here and other published findings, the proposed method shows substantial tractability in being able to effectively combine the results from validated musculoskeletal rigid body models with patient-specific derived finite element models for novel exertions. Future efforts should be directed in better utilizing available methods for defining subject-specific geometry used for the finite element model as well as assessing the effect of the slight nodal displacements imparted to the rigid body model on the simulated muscle forces. Additionally, an optimization procedure to best match the derived patient bone geometry to the rigid body model to achieve an optimal match would be beneficial. Future applications of the presented methodology should also focus on utilizing the results from the finite element model (i.e. displacements) to drive/adapt the inverse dynamics motion for accurate simulations of more flexible internal structures. It is hoped that the tool developed in the present work can be utilized to further develop coupled models utilizing the best aspects from rigid body dynamics and finite element modeling simulations.

References

Anderson, A.E., Ellis, B.J. and Weiss, J.A. (2007), "Verification, validation and sensitivity studies in computational biomechanics", *Computer Methods in Biomechanics and Biomedical Engineering*, Vol. 10 No. 3, pp. 171-84.

Anderson, F.C. and Pandy, M.G. (2001), "Static and dynamic optimization solutions for gait are practically equivalent", *Journal of Biomechanics*, Vol. 34 No. 2, pp. 153-61.

Bergmann, G., Graichen, F. and Rohlmann, A. (1995), "Is staircase walking a risk for the fixation of hip implants?", *Journal of Biomechanics*, Vol. 28 No. 5, pp. 535-53.

Bitsakos, C., Kerner, J., Fisher, I. and Amis, A.A. (2005), "The effect of muscle loading on the simulation of bone remodelling in the proximal femur", *Journal of Biomechanics*, Vol. 38 No. 1, pp. 133-9.

Brand, R.A., Pedersen, D.R. and Friederich, J.A. (1986), "The sensitivity of muscle force predictions to changes in physiologic cross-sectional area", *Journal of Biomechanics*, Vol. 19 No. 8, pp. 589-96.

Brand, R.A., Crowninshield, R.D., Wittstock, C.E., Pedersen, D.R., Clark, C.R. and van Krieken, F.M. (1982), "A model of lower extremity muscular anatomy", *Journal of Biomechanical Engineering*, Vol. 104 No. 4, pp. 304-10.

Cody, D.D., Gross, G.J., Hou, F.J., Spencer, H.J., Goldstein, S.A. and Fyhrie, D.P. (1999), "Femoral strength is better predicted by finite element models than QCT and DXA", *Journal of Biomechanics*, Vol. 32 No. 10, pp. 1013-20.

Crawford, R., Cann, C. and Keaveny, T. (2003), "Finite element models predict in vitro vertebral body compressive strength better than quantitative computed tomography", *Bone*, Vol. 33 No. 4, pp. 744-50.

Cristofolini, L., Viceconti, M., Cappello, A. and Toni, A. (1996), "Mechanical validation of whole bone composite femur models", *Journal of Biomechanics*, Vol. 29 No. 4, pp. 525-35.

Damsgaard, M., Rasmussen, J., Christensen, S.T., Surma, E. and de Zee, M. (2006), "Analysis of musculoskeletal systems in the anybody modeling system", *Simulation Modelling Practice and Theory*, Vol. 14 No. 8, pp. 1100-11.

Doblare, M. and Garcia, J.M. (2001), "Application of an anisotropic bone-remodelling model based on a damage-repair theory to the analysis of the proximal femur before and after total hip replacement", *Journal of Biomechanics*, Vol. 34 No. 9, pp. 1157-70.

Doblare, M. and Garcia, J.M. (2003), "On the modelling bone tissue fracture and healing of the bone tissue", *Acta Cient Venez*, Vol. 54 No. 1, pp. 58-75.

Duda, G., Heller, M., Albinger, J., Schulz, O., Schneider, E. and Claes, L. (1998), "Influence of muscle forces on femoral strain distribution", *Journal of Biomechanics*, Vol. 31 No. 9, pp. 841-6.

Erdemir, A., McLean, S., Herzog, W. and van den Bogert, A.J. (2007), "Model-based estimation of muscle forces exerted during movements", *Clinical Biomechanics*, Vol. 22 No. 2, pp. 131-54.

Frost, H. (1999), "Why do bone strength and mass in aging adults become unresponsive to vigorous exercise? Insights of the Utah paradigm", *Journal of Bone and Mineral Metabolism*, Vol. 17 No. 2, pp. 90-7.

Grujicic, M., Pandurangan, B., Arakere, G., Bell, W.C., He, T. and Xie, X. (2009), "Seat-cushion and soft-tissue material modeling and a finite element investigation of the seating comfort for passenger-vehicle occupants", *Materials and Design*, Vol. 30 No. 10, pp. 4273-85.

Grujicic, M., Pandurangan, B., Xie, X., Gramopadhye, A.K., Wagner, D. and Ozen, M. (2010a), "Musculoskeletal computational analysis of the influence of car-seat design/adjustments on long-distance driving fatigue", *International Journal of Industrial Ergonomics*, Vol. 40 No. 3, pp. 345-55.

Grujicic, M., Arakere, G., Xie, X., LaBerge, M., Grujicic, A., Wagner, D.W. and Vallejo, A. (2010b), "Design-optimization and material selection for a femoral-fracture fixation-plate implant", *Journal of Materials and Design*, Vol. 31 No. 7, pp. 3463-73.

Grujicic, M., Xie, X., Arakere, G., Grujicic, A., Wagner, D.W. and Vallejo, A. (2010c), "Design-optimization and material selection for a proximal radius fracture-fixation implant", *Journal of Materials Engineering and Performance*, Vol. 19 No. 8, pp. 1090-103.

Grujicic, A., Laberge, M., Xie, X., Arakere, G., Pandurangan, B., Grujicic, M., Jeray, K.J. and Tanner, S.L. (2010d), "Computational investigation of the efficacy of a nail-type, a plate-type proximal femoral-fracture fixation implant", *Journal of Engineering in Medicine* (submitted for publication).

Heaney, R.P. (2003), "Is the paradigm shifting?", *Bone*, Vol. 33 No. 4, pp. 457-65.

Heiner, A.D. and Brown, T.D. (2001), "Structural properties of a new design of composite replicate femurs and tibias", *Journal of Biomechanics*, Vol. 34 No. 6, pp. 773-81.

Hernandez, C. and Keaveny, T. (2006), "A biomechanical perspective on bone quality", *Bone*, Vol. 39 No. 6, pp. 1173-81.

Huiskes, R. and van Rietbergen, B. (1995), "Preclinical testing of total hip stems: the effects of coating placement", *Clinical Orthopaedics*, Vol. 319, pp. 64-76.

Jacobs, C.R., Simo, J.C., Beaupre, G.S. and Carter, D.R. (1997), "Adaptive bone remodeling incorporating simultaneous density and anisotropy considerations", *Journal of Biomechanics*, Vol. 30 No. 6, pp. 603-13.

Keyak, J.H. (2001), "Improved prediction of proximal femoral fracture load using nonlinear finite element models", *Medical Engineering & Physics*, Vol. 23 No. 3, pp. 165-73.

Keyak, J.H. and Falkinstein, Y. (2003), "Comparison of in situ and in vitro ct scan-based finite element model predictions of proximal femoral fracture load", *Medical Engineering & Physics*, Vol. 25 No. 9, pp. 781-7.

Keyak, J.H., Skinner, H.B. and Fleming, J.A. (2001), "Effect of force direction on femoral fracture load for two types of loading conditions", *Journal of Orthopaedic Research*, Vol. 19 No. 4, pp. 539-44.

Koopman, B., Grootenboer, H.J. and de Jongh, H.J. (1995), "An inverse dynamics model for the analysis, reconstruction and prediction of bipedal walking", *Journal of Biomechanics*, Vol. 28 No. 11, pp. 1369-76.

Lee, B.-H., Kim, J.K., Kim, Y.D., Choi, K. and Lee, K.H. (2004), "In vivo behavior and mechanical stability of surface modified titanium implants by plasma spray coating and chemical treatments", *Journal of Biomedical Materials Research Part A*, Vol. 69 No. 2, pp. 279-85.

Lengsfeld, M., Schmitt, J., Alter, P., Kaminsky, J. and Leppek, R. (1998), "Comparison of geometry-based and CT voxelbased finite element modelling and experimental validation", *Medical Engineering & Physics*, Vol. 20 No. 7, pp. 515-22.

Lotz, J.C., Gerhart, T.N. and Hayes, W.C. (1991), "Mechanical properties of metaphyseal bone in the proximal femur", *Journal of Biomechanics*, Vol. 24 No. 5, pp. 317-29.

Mann, K.A., Bartel, D.L. and Ayers, D.C. (1997), "Influence of stem geometry on mechanics of cemented femoral hip components with a proximal bond", *Journal of Orthopaedic Research*, Vol. 15 No. 5, pp. 700-6.

Peng, L., Bai, J., Zeng, X. and Zhou, Y. (2006), "Comparison of isotropic and orthotropic material property assignments on femoral finite element models under two loading conditions", *Medical Engineering & Physics*, Vol. 28 No. 3, pp. 227-33.

Post, D. (2004), "The coming crisis in computational science", *Proceedings of the IEEE International Conference on High Performance Computer Architecture: Workshop on Productivity and Performance in High-end Computing, Madrid, Spain*.

Rasmussen, J. (2006), "Gait modeling", available at: www.anybodytech.com/196.html.

Rasmussen, J., Damsgaard, M., Egidigus, S., Christensen, S.T. and de Zee, M. (2003), "Designing a general software system for musculoskeletal analysis", paper presented at the IX International Symposium on Computer Simulation in Biomechanics, Sydney, Australia.

Ren, L., Jones, R.K. and Howard, D. (2007), "Predictive modelling of human walking over a complete gait cycle", *Journal of Biomechanics*, Vol. 40 No. 7, pp. 1567-74.

Schileo, E., Taddei, F., Malandrino, A., Cristofolini, L. and Viceconti, M. (2007), "Subject-specific finite element models can accurately predict strain levels in long bones", *Journal of Biomechanics*, Vol. 40 No. 13, pp. 2982-9.

Schneider, E., Michel, M.C., Genge, M., Zuber, K., Ganz, R. and Perren, S.M. (2001), "Loads acting in an intramedullary nail during fracture healing in the human femur", *Journal of Biomechanics*, Vol. 34 No. 7, pp. 849-57.

Shim, V.B., Pitto, R.P., Streicher, R.M., Hunter, P.J. and Anderson, I.A. (2007), "The use of sparse CT datasets for auto-generating accurate FE models of the femur and pelvis", *Journal of Biomechanics*, Vol. 40 No. 1, pp. 26-35.

Speirs, A., Heller, M., Duda, G. and Taylor, W. (2007), "Physiologically based boundary conditions in finite element modelling", *Journal of Biomechanics*, Vol. 40 No. 10, pp. 2318-23.

Stokes, I.A.F. and Gardner-Morse, M. (2004), "Muscle activation strategies and symmetry of spinal loading in the lumbar spine with scoliosis", *Spine*, Vol. 29 No. 19, pp. 2103-7.

Stülpner, M., Reddy, B., Starke, G. and Spirakis, A. (1997), "A three-dimensional finite analysis of adaptive remodelling in the proximal femur", *Journal of Biomechanics*, Vol. 30 No. 10, pp. 1063-6.

Taddei, F., Schileo, E., Helgason, B., Cristofolini, L. and Viceconti, M. (2007), "The material mapping strategy influences the accuracy of CT-based finite element models of bones: an evaluation against experimental measurements", *Medical Engineering & Physics*, Vol. 29 No. 9, pp. 973-9.

Taylor, M.E., Tanner, K.E., Freeman, M.A.R. and Yettram, A.L. (1996), "Stress and strain distribution within the intact femur: compression or bending?", *Medical Engineering & Physics*, Vol. 18 No. 2, pp. 122-31.

Vaughan, C.L., Davis, B.L. and O'Connor, J.C. (1992), *Dynamics of Human Gait*, Human Kinetics Publishers, Champaign, IL.

Viceconti, M., Ansaloni, M., Baleani, M. and Toni, A. (2003), "The muscle standardized femur: a step forward in the replication of numerical studies in biomechanics", *Proceedings of the Institution of Mechanical Engineers, Part H: Journal of Engineering in Medicine*, Vol. 217 No. 2, pp. 105-10.

Viceconti, M., Olsen, S., Nolte, L. and Burton, K. (2005), "Extracting clinically relevant data from finite element simulations", *Clinical Biomechanics*, Vol. 20 No. 5, pp. 451-4.

Wirtz, D.C., Schiffers, N., Pandorf, T., Radermacher, K., Weichert, D. and Forst, R. (2000), "Critical evaluation of known bone material properties to realize anisotropic FE-simulation of the proximal femur", *Journal of Biomechanics*, Vol. 33, pp. 1325-30.

Yosibash, Z., Trabelsi, N. and Milgrom, C. (2007), "Reliable simulations of the human proximal femur by high-order finite element analysis validated by experimental observations", *Journal of Biomechanics*, Vol. 40 No. 16, pp. 3688-99.

Further reading

Keyak, J.H. and Rossi, S. (2000), "Prediction of femoral fracture load using finite element models: an examination of stress-and strain-based failure theories", *Journal of Biomechanics*, Vol. 33 No. 2, pp. 209-14.

Silver-Thorn, M.B., Steege, J.W. and Childress, D.S. (1996), "A review of prosthetic interface stress investigations", *Journal of Rehabilitation Research and Development*, Vol. 33 No. 3, pp. 253-66.

About the authors

David W. Wagner works for Ozen Engineering Inc. as Research Scientist. His specialization is in the field of combined musculoskeletal dynamics and finite element analysis.

Kaan Divringi works for Ozen Engineering Inc. as a Project Engineer. His research interests include computer aided-engineering (CAE) analysis of orthopedic implants.

Can Ozcan works for Ozen Engineering Inc. and is presently the Director of Engineering. His research is focused CAE analysis of orthopedic implants and other prosthetic devices.

M. Grujicic is the Wilfred P. and Helen S. Tiencken Professor of Mechanical Engineering at Clemson University, South Carolina. His research interests are in the field of computational materials development and engineering analysis. M. Grujicic is the corresponding author and can be contacted at: mica.grujicic@ces.clemson.edu

B. Pandurangan is a post-doctoral fellow in the Mechanical Engineering Department at Clemson University, South Carolina. His research focuses on computational materials engineering and finite element analysis of prosthetic devices.

A. Grujicic is an under-graduate student in the Bioengineering Department at Clemson University, South Carolina. Her research interests include computational biomechanics and analysis of implant devices.